International Journal of Thermal Sciences 49 (2010) 428–442

Contents lists available at ScienceDirect

International Journal of Thermal Sciences

journal homepage: www.elsevier.com/locate/ijts

Parametric study of turbulent slot-jet impingement heat transfer from concave cylindrical surfaces

M.A.R. Sharif*, K.K. Mothe

Aerospace Engineering and Mechanics Department, The University of Alabama, Tuscaloosa, AL 35487-0280, USA

ARTICLE INFO

Article history:
Received 3 December 2008
Received in revised form
19 July 2009
Accepted 20 July 2009
Available online 14 August 2009

Keywords:
Numerical simulation
Slot-jet impingement
Concave surface
RNG k–ε model

ABSTRACT

Numerical investigation of convective heat transfer process from concave cylindrical surfaces due to turbulent slot-jet impingement is performed. Constant heat flux condition is specified at the concave surfaces. The flow and thermal fields in the vicinity of the surfaces are computed using the RNG k–ε turbulence model with a two-layer near wall treatment. Parametric studies are carried out for various jet-exit Reynolds numbers, surface curvature, and nozzle-to-surface spacing. Results presented include streamlines, isotherms, velocity and temperature profiles in the wall-jet region, and the local Nusselt number distribution on the impingement concave wall for various parameter values in the study. The results indicate that while the jet-exit Reynolds number and the surface curvature have a significant effect on the heat transfer process, it is relatively insensitive to the jet-to-target spacing. A correlation for the average Nusselt number at the concave surface as a function of the parameters considered in the study is also derived.

1. Introduction

Due to high rates of localized heat transfer, impinging jet flows are employed in a wide variety of applications of practical interest, such as surface coating and cleaning, cooling of electronic components, metal cutting and forming, fire testing and building materials, turbine blade cooling, drying of textiles, veneer, paper and film materials, aircraft wing leading edge heating for anti-icing application, etc. Even though the flow geometry is simple in jet impingement heat transfer problems, the physics of the flow is very complex due to the shear layer development at the free jet and wall jet boundaries, boundary layer development at the impingement surface, and very high streamline curvature near the impingement location. The flow physics of jets impinging on flat surfaces is significantly altered when the impingement occurs on a curved surface. The surface curvature has a strong effect on the overall flow as well as in the wall jet development in the circumferential direction due to the additional streamline curvature and associated centrifugal and Coriolis forces. The surface curvature also has a strong effect on the turbulent boundary layer development. The heat transfer rate for impingement on curved surfaces is found to increase by an order of 20% by various researchers. However, the details of the effects of surface curvature are not well understood at present even though in many practical engineering applications jet impingement occurs on curved surfaces.

Numerical modeling of jet impingement on curved surfaces is very challenging due to the complex interaction of the flow entrainment and strong streamline curvature. The choice of turbulence models is also very crucial in numerical analysis of impinging jet heat transfer process specifically due to the over-prediction of kinetic energy generation at the impingement region by various eddy-viscosity models.

There have been numerous studies conducted in the past related to jet impingement flow and heat transfer, most of which considered impinging jet flow on flat surfaces. While impingement on flat surfaces has practical significance for numerous applications, many other instances of jet impingement are onto surfaces with a degree of curvature, such as turbine rotor blade leading edge cooling and airfoil leading edge heating for anti-icing applications. A heat transfer correlation as a function of the geometric and flow parameters is very desirable for the design of the cooling/heating system in these applications. There has not been much investigation into the flow of jets impinging upon curved surfaces. In general, the limited work that has been done mainly focuses on experimental heat and/or mass transfer measurements and their theoretical interpretation. These results show significant differences in the flow dynamics and heat transfer from the data for planar impingement surfaces. Among the recent experimental

* Corresponding author. Tel.: +1 205 348 8052; fax: +1 205 348 7240.
E-mail address: msharif@eng.ua.edu (M.A.R. Sharif).

1290-0729/$ – see front matter © 2009 Elsevier Masson SAS. All rights reserved.
doi:10.1016/j.ijthermalsci.2009.07.017

Nomenclature

a	inward normal distance from the concave cylindrical surface, m
B	slot-jet width for impingement on concave surface case, m
c_p	specific heat at constant pressure, N m/kg K
D	diameter of the concave surface, m
h	distance of the impingement surface from the jet-exit, m
k	turbulent kinetic energy, m^2/s^2 or thermal conductivity of the fluid, W/m K
n	normal distance from wall, m
Nu	Nusselt number
P	mean pressure, Pa
Pr	Prandtl number, $c_p\mu/k$
q_w	heat flux at the impingement surface, W/m^2
r	distance along the jet axis from the exit of the jet, m
s	arc distance along the concave surface, m
Re	Reynolds number at the jet exit, $\rho U_j(2B)/\mu$
Re_y	Turbulent Reynolds number, $\rho n\sqrt{k}/\mu$
T	mean temperature, K
T_j	jet-exit temperature, K
T_w	impingement surface temperature, K
T'	fluctuating temperature, K
u_j'	fluctuating velocity component, m/s
U_i	mean velocity component, m/s
U_j	jet-exit velocity, m/s
x_i	spatial coordinates

Greek symbols

ε	time rate of turbulent kinetic energy dissipation
μ	dynamic viscosity
μ_t	turbulent or eddy viscosity
ρ	fluid density
ω	specific dissipation rate of turbulent kinetic energy

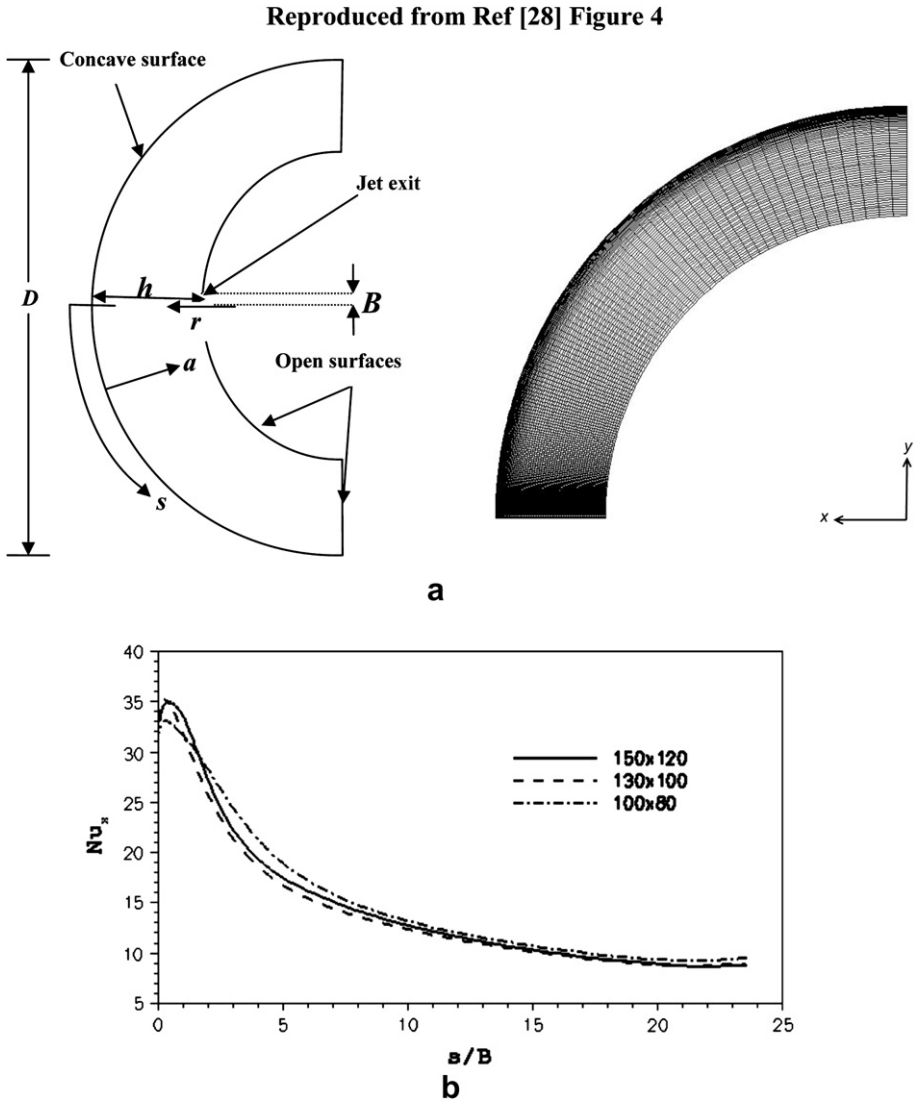

Fig. 1. (a) Schematic diagram of the slot-jet impingement on a concave cylindrical surface and a sample mesh, (b) representative grid independence study for impingement on concave surface.

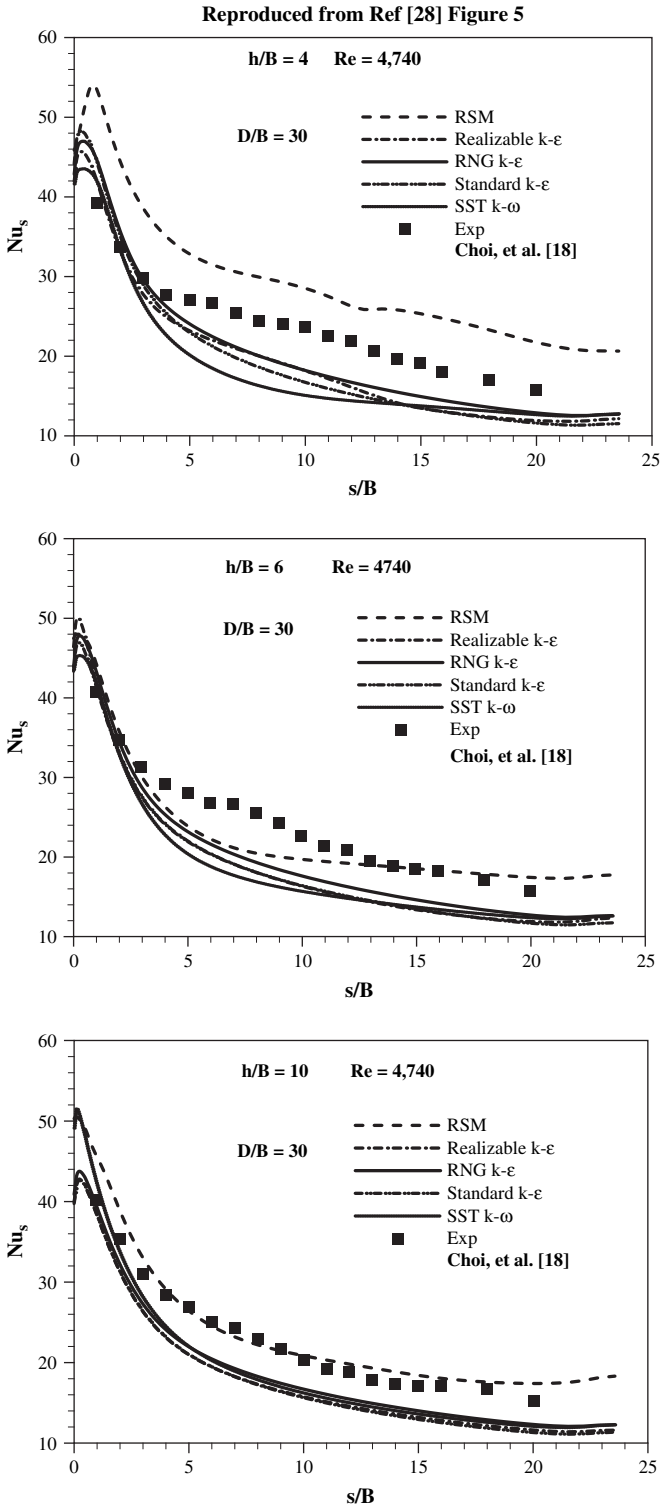

Fig. 2. Comparison of the predicted local Nusselt number distribution along the concave surface against the experimental data of Choi et al. [18].

investigation of jet impingement on curved surfaces the works of Bunker and Metzger [1], Gau and Chung [2], Lee et al. [3,4], Kornblum and Goldstein [5], Cornanro et al. [6], Yang et al. [7], Cornaro et al. [8], Kayansayan and Kucuka [9], Chan et al. [10], Iacovides et al. [11], Eren et al. [12], Lee et al. [13], Chang et al. [14], Eren et al. [15], Hu and Zhang [16], and Fenot et al. [17] can be mentioned. These studies include the cases of impingement on concave and convex surfaces. Kayansayan and Kucuka [9] performed experimental investigation for impingement cooling of semi-cylindrical concave channels by slot-jet. Their jet Reynolds number ranged from 200 to 11,000, while the normalized jet-to-impingement surface spacing ranged from 2.2 to 4.2. Thus their flow domain was confined by two concentric semi-cylindrical isothermal walls and the hot impingement wall was located within the potential core of the jet. They also performed numerical investigation for laminar flow for a jet Reynolds number up to 600. They did not perform computations for turbulent flow due to lack of suitable turbulence model. Eren et al. [15] conducted experimental investigation for slot-jet impingement heat transfer from slightly concave and convex unconfined surfaces at constant heat flux condition. Their Reynolds number ranged from 8617 to 15,415 and the jet-to-impingement surface distance was kept constant at 8. Choi et al. [18] experimentally investigated slot-jet impingement cooling of semi-circular concave surfaces and presented the thermal and hydrodynamic data for different Reynolds numbers and nozzle-to-surface distances. Reports of numerical investigation of turbulent jet impingement heat transfer from curved surfaces is not plentiful in the literature. Yang and Hwang [19] numerically investigated the hydrodynamics of turbulent slot-jet impingement on convex semi-cylindrical surfaces without any heat transfer consideration. Souris and Liakos [20] have done numerical studies on impingement cooling on concave cylindrical surfaces using the standard k–ε model and the Reynolds stress transport model along with the non-equilibrium wall function [21] for both models. They compared their predictions with the experimental data of Choi et al. [18] and found a satisfying agreement between the numerical prediction and experimental data using both turbulence models. Kayansayan and Kucuka [9] carried out numerical investigation for confined slot-jet impingement from concave cylindrical surface similar to their experimental configuration. Frageau et al. [22] computed the flow and heat transfer due to an array of circular jets impinging on concave surface for aircraft wing leading edge anti-icing application. Hu and Zhang [16] conducted numerical investigation in addition to the experimental measurement for circular water jet impingement heat transfer from a convex hemispherical surface. They, however, did not report which turbulence model was used in the computation, if any. Craft et al. [23] computed the flow and heat transfer from a row of round jets impinging onto a concave semi-circular surface employing linear and non-linear eddy viscosity turbulence models. Kumar and Prasad [24] numerically investigated the flow and heat transfer from a row of circular jets impinging on a concave cylindrical surface using the Fluent CFD code and the SST k–ω turbulence model. Wrachien and Lorenzini [25] have reported empirical/analytical and experimental results for jet modeling in the context of sprinkler irrigation jet sprays.

In the present work, a parametric study of the slot-jet impingement on unconfined concave cylindrical surfaces is conducted for a wide range of flow and geometric parameters such as jet-exit Reynolds number, jet-to-surface spacing, and relative surface curvature. This particular geometric configuration is chosen based on the experimental setup of Choi et al. [18] so that the code validation can be performed against their experimental data. The computations in this study are performed using the Fluent version 6.3 commercial flow solver code [26]. The results of the parametric study are presented in terms of the streamline and isotherm plots, Nusselt number at the heated surface, and the velocity profiles across the shear layer in the wall-jet region. A correlation for the average Nusselt number for impinging flows over concave surfaces has been derived as a function of the parameters, which can be used by the industry.

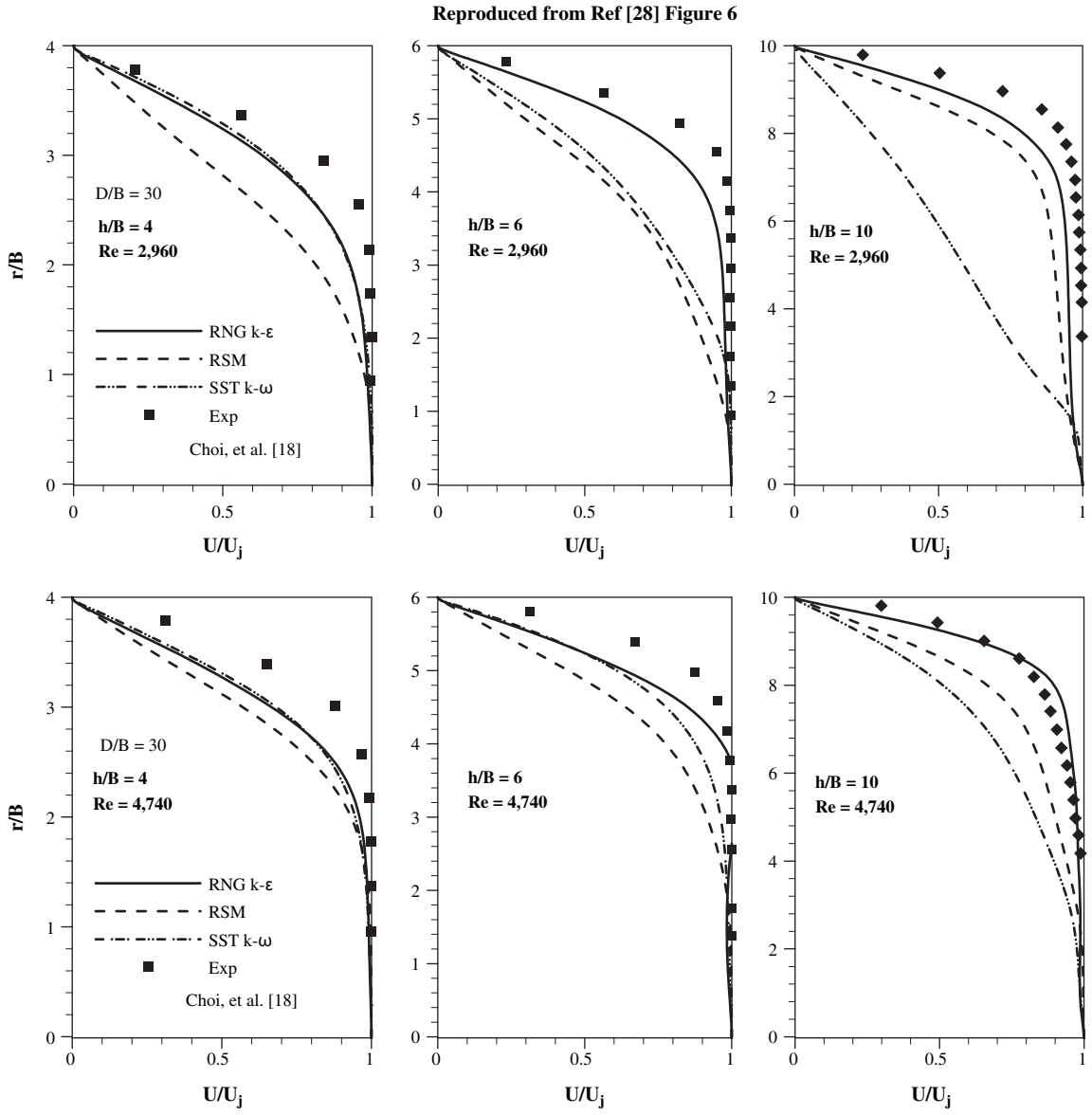

Fig. 3. Comparison of the predicted mean axial velocity variation along the jet centerline against experimental data [18].

2. Mathematical formulation

The Reynolds averaged mass, momentum, and energy conservation equations for the steady incompressible flow, neglecting the viscous dissipation, are given as

$$\frac{\partial U_i}{\partial x_i} = 0 \tag{1}$$

$$\rho U_j \frac{\partial U_i}{\partial x_j} = -\frac{\partial P}{\partial x_i} + \frac{\partial}{\partial x_j}\left[\mu\left(\frac{\partial U_i}{\partial x_j} + \frac{\partial U_j}{\partial x_i}\right) - \rho\overline{u_i' u_j'}\right] \tag{2}$$

$$\rho U_j \frac{\partial T}{\partial x_j} = \frac{\partial}{\partial x_j}\left[\frac{\mu}{\mathrm{Pr}}\frac{\partial T}{\partial x_j} - \rho\overline{T' u_j'}\right] \tag{3}$$

where P, T, and U_i are the mean pressure, temperature, and velocity components, respectively, T' and u_i' are the fluctuating temperature and velocity components, respectively, x_i is the coordinate direction, and ρ, μ, and Pr are the fluid density, dynamic viscosity, and Prandtl number, respectively. The turbulent Reynolds stresses, $-\rho\overline{u_i' u_j'}$, in Eq. (2) are calculated by an appropriate turbulence model for closure. In the eddy-viscosity models, the turbulent stresses are assumed to be linearly proportional to the strain rate and are calculated as

$$-\rho\overline{u_i' u_j'} = \mu_t\left(\frac{\partial U_i}{\partial x_j} + \frac{\partial U_j}{\partial x_i}\right) - \frac{2}{3}\rho k\delta_{ij} \tag{4}$$

where μ_t is the turbulent eddy viscosity, δ_{ij} is the Kronecker delta, and $k = u_i' u_i'/2$ is the kinetic energy of turbulence. The eddy viscosity, in turn, is obtained from an empirical formula as a function of the kinetic energy of turbulence and the turbulent length scale. In the standard k–ε model developed by Launder and Spalding [27] the transport equations for the kinetic energy of turbulence, k, and the time rate of dissipation of k, which is defined as $\varepsilon = (\mu/\rho)\overline{(\partial u_i'/\partial x_j)(\partial u_j'/\partial x_i)}$ are solved. The turbulent length scale, l, is related to k and ε as $l = k^{3/2}/\varepsilon$. Once k and ε are obtained from the solution of their respective transport equations, the eddy viscosity is calculated as $\mu_t = \rho C_\mu k^2/\varepsilon$ where C_μ is an empirical constant. The transport equations for k and ε are given as

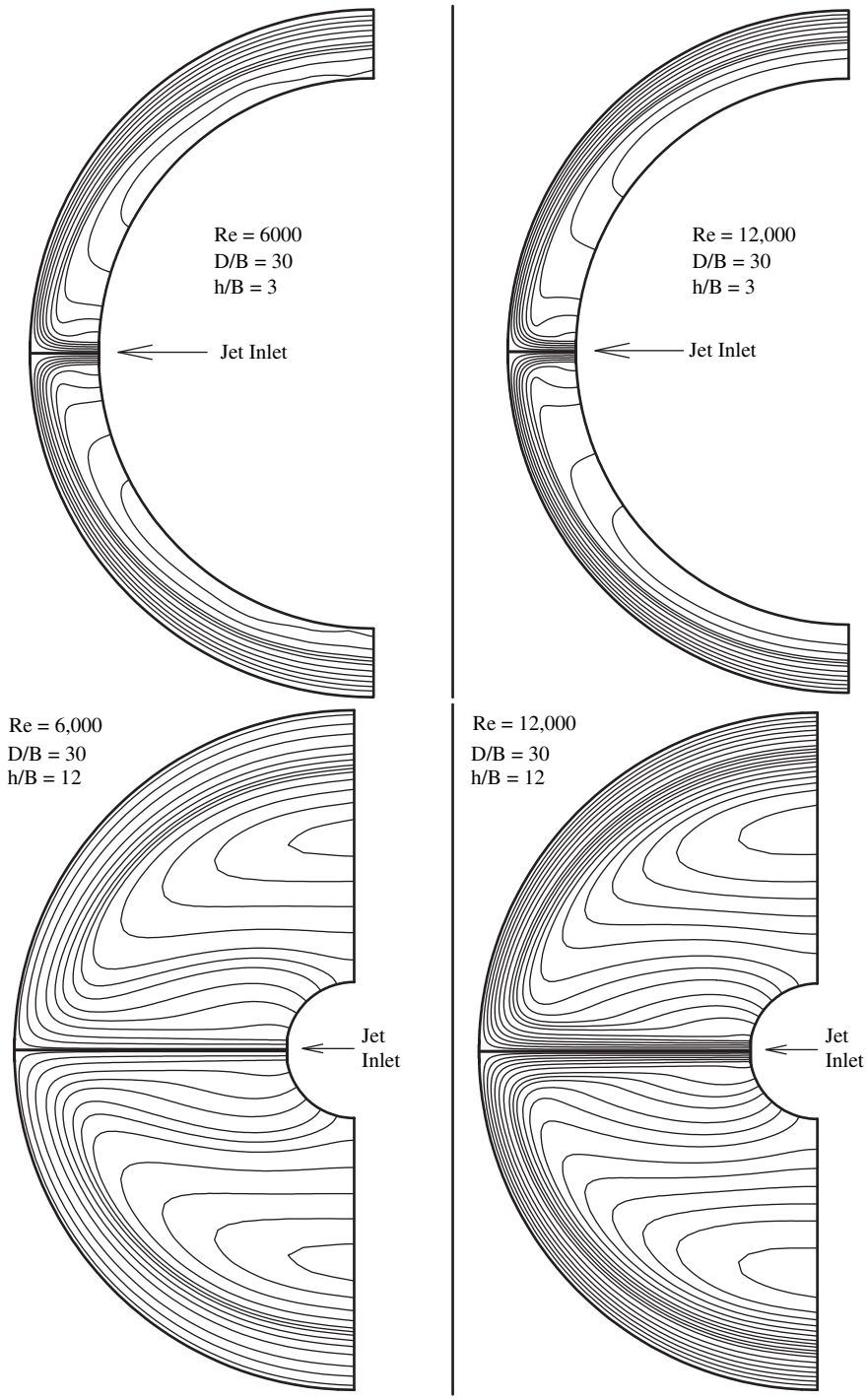

Fig. 4. Some representative streamline plots in the flow domain.

$$\rho U_j \frac{\partial k}{\partial x_j} = \frac{\partial}{\partial x_j}\left[\left(\mu + \frac{\mu_t}{\sigma_k}\right)\frac{\partial k}{\partial x_j}\right] + P_k - \rho\varepsilon \tag{5}$$

$$\rho U_j \frac{\partial \varepsilon}{\partial x_j} = \frac{\partial}{\partial x_j}\left[\left(\mu + \frac{\mu_t}{\sigma_\varepsilon}\right)\frac{\partial \varepsilon}{\partial x_j}\right] + C_{1\varepsilon}\frac{\varepsilon}{k}P_k - C_{2\varepsilon}\rho\frac{\varepsilon^2}{k} \tag{6}$$

where

$$P_k = \left[\mu_t\left(\frac{\partial U_i}{\partial x_j} + \frac{\partial U_j}{\partial x_i}\right) - \frac{2}{3}\rho k\delta_{ij}\right]\frac{\partial U_i}{\partial x_j} \tag{7}$$

In a recent study by the present authors [28] the performance of several eddy-viscosity turbulence models in the prediction of heat transfer due to jet impingement on plane and curved surfaces was evaluated against experimental data. It was found that the RNG k–ε turbulence model [29] along with the two-layer near-wall treatment produced the most satisfactory thermal as well as hydrodynamic flow field prediction compared to the experimental data. For this reason the RNG k–ε model is employed in the present

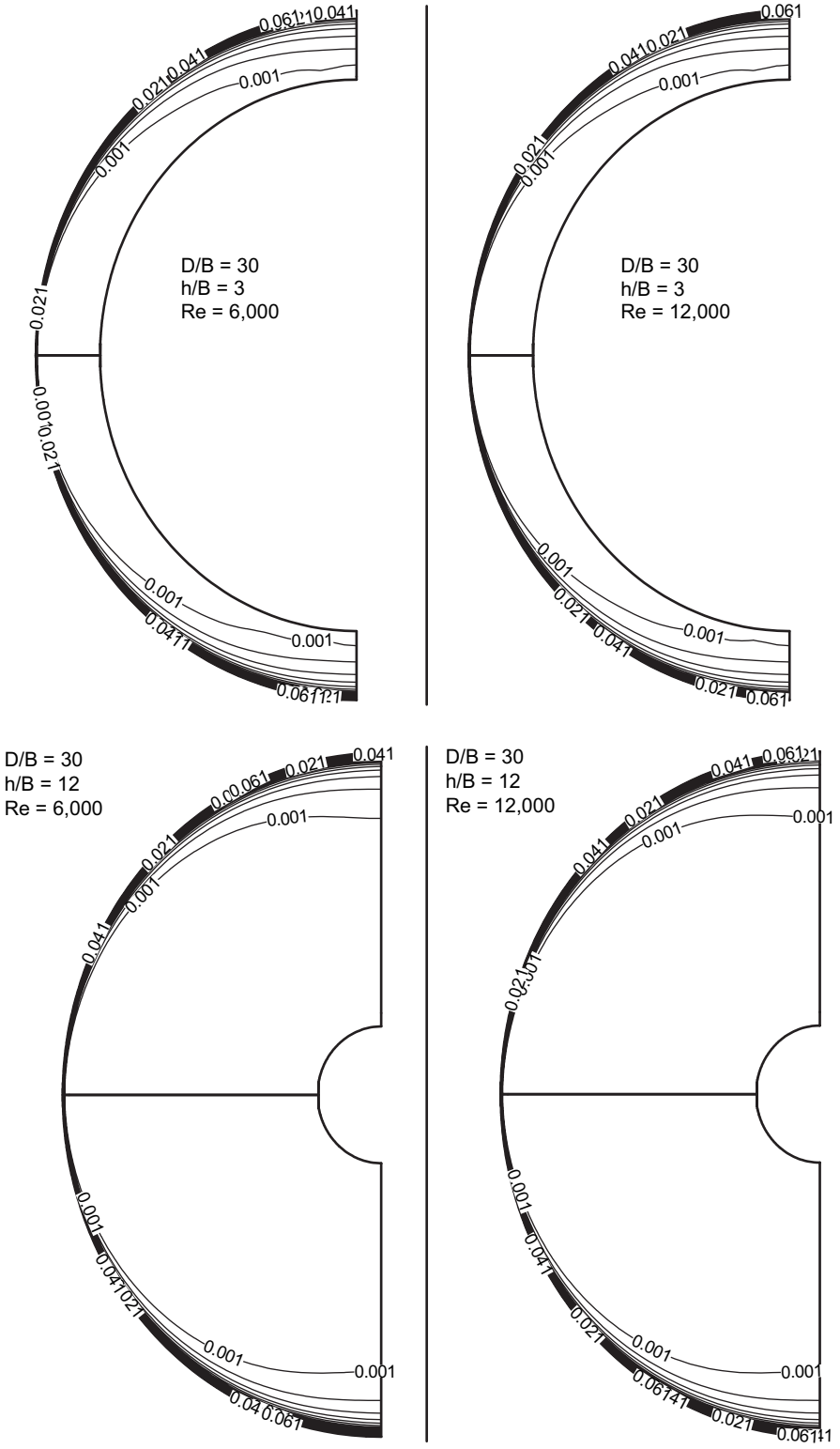

Fig. 5. Some representative isotherm plots in the flow domain.

parametric study for impingement heat transfer from concave cylindrical surfaces. The RNG-based k–ε turbulence model is derived from the instantaneous Navier–Stokes equation, using a mathematical technique called Re-Normalization Group (RNG) method. The analytical derivation results in a model having similar transport equations but with constants different from those in the standard k–ε model, and an additional term in the right hand side of the transport equation for ε which is given as

$$R_\varepsilon = -\frac{C_\mu \eta^3 (1-\eta/\eta_0)}{1+\beta\eta^3}\frac{\varepsilon^2}{k} \tag{8}$$

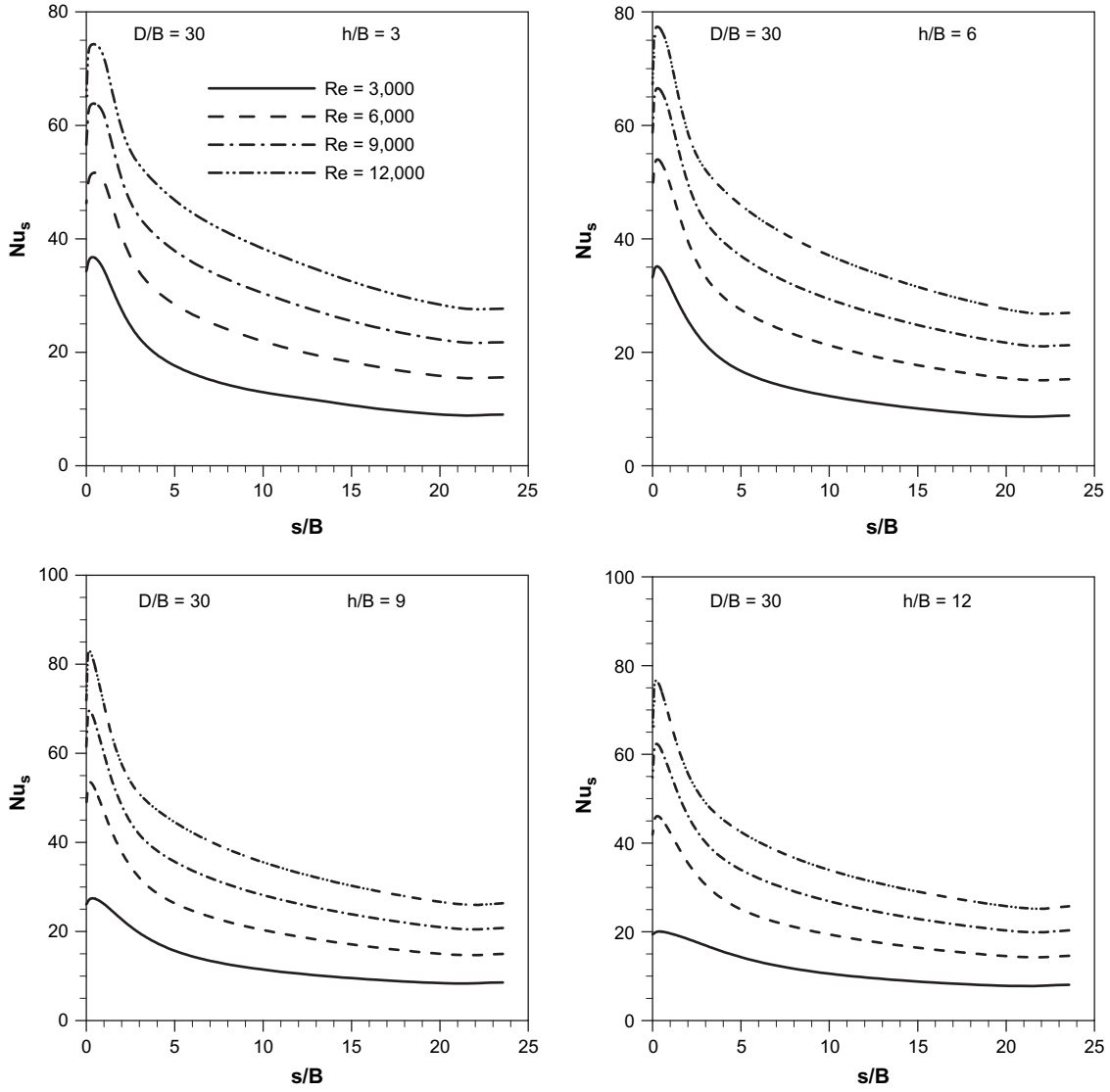

Fig. 6. Local Nusselt number variation along the heated concave surface for different Reynolds numbers for $D/B = 30$.

where $\eta = Sk/\varepsilon$, $S = (2S_{ij}S_{ij})^{1/2}$, and $S_{ij} = (\partial u_i/\partial x_j + \partial u_j/\partial x_i)/2$. This modification significantly improves the accuracy for rapidly strained flows. The various model constants in the RNG k–ε model are given as $C_{1\varepsilon} = 1.42$, $C_{2\varepsilon} = 1.68$, $C_\mu = 0.0845$, $\sigma_k = 0.7194$, $\sigma_\varepsilon = 0.7194$, $\eta_0 = 4.38$, and $\beta = 0.012$. These constants are explicitly derived analytically in the RNG procedure except for β which is the only empirical constant. While the standard k–ε model is a high Reynolds number model, the RNG theory provides an analytically-derived differential formula for the effective viscosity that accounts for low Reynolds number effects. Effective use of this feature, however, depends on an appropriate treatment of the near-wall region in terms of mesh refinement.

The near-wall treatment employed in this study involves a two-layer approach. The boundary layer is subdivided into a near-wall viscosity affected region where the turbulent Reynolds number, Re_y, is less than 200 and a fully turbulent region where $Re_y > 200$. The turbulent Reynolds number is defined as $Re_y = \rho n\sqrt{k}/\mu$ where n is the normal distance from the wall. In the fully turbulent region, the RNG k–ε model is employed whereas in the near-wall region the one-equation model of Wolfstein [30] is used. In this one-equation model the transport equation for k is retained but ε and μ_t is calculated using algebraic equations. The values of ε and μ_t across the interface of the two layers are blended smoothly using some blending parameter. The details of the two-layer near-wall treatment can be found in the Fluent user guide [26].

The turbulent heat flux, $-\rho\overline{T'u'_j}$, in Eq. (3) is obtained according to the simple gradient diffusion hypothesis (SGDH) [31] as

$$-\rho\overline{T'u'_j} = \frac{\mu_t}{\sigma_t}\left(\frac{\partial T}{\partial x_j}\right) \tag{9}$$

where σ_t is the turbulent Prandtl number whose value is taken as 0.85.

3. Numerical procedure

The flow domain is divided into many small finite volumes with an unstructured mesh. A collocated arrangement for the placement of the flow variables is used in the mesh system. The nonlinear conservation equations for mass, momentum, and energy and other transport equations are integrated over each of the finite volume to yield sets of linear algebraic equations. These sets of linear algebraic equations are then solved sequentially using an iterative method such as the line successive over relaxation

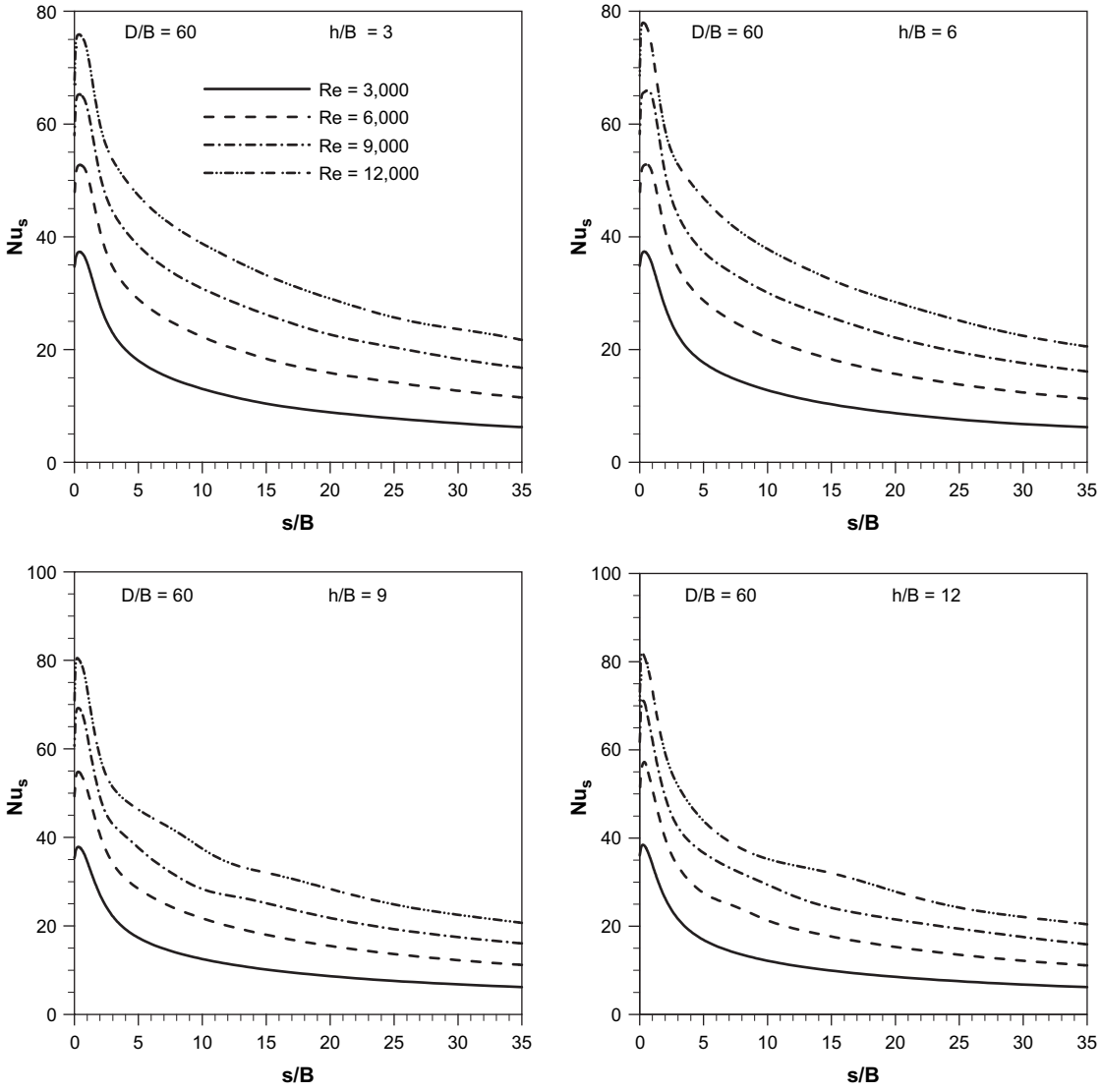

Fig. 7. Local Nusselt number variation along the heated concave surface for different Reynolds numbers for $D/B = 60$.

method. The SIMPLE algorithm [32] is used for pressure–velocity coupling. The convective fluxes have been calculated using the second-order upwind scheme while the diffusive fluxes have been calculated using the central difference scheme. The convergence is assumed when the value of the scaled residual of continuity, momentum and energy equations is less than 10^{-6}. Convergence has also been monitored by plotting the average Nusselt number on the impingement surface until the variation of the average Nusselt number levels off with iteration.

4. Problem set up

4.1. Geometry of the problem

Fig. 1(a) (reproduced from [28], Fig. 4) shows the schematic diagram of the impinging slot-jet on a semi-circular concave surface which closely resembles the experimental conditions of Choi et al. [18]. The jet is unconfined, meaning the two vertical plane surfaces and the circular surfaces around the jet bounding the domain shown in the diagram are open. The variable '*a*' in the sketch represents the inward radial distance from the impingement wall, the variable '*r*' represents the distance along the jet axis from the jet exit, while the variable '*s*' represents the distance along the circumferential direction from the impingement point.

The experimental conditions [18] consisted of a slot-jet with 5 mm width (B) used to produce an air jet impinging onto a semi-circular concave surface with a diameter (D) of 150 mm, on which a constant heat flux q_w of 5000 W/m^2 was applied. Measurements were taken for three jet-to-target spacing (h/B) values of 4, 6, and 10. In the first case ($h/B = 4$), the target surface was inside the potential core whereas in the second case ($h/B = 6$) and the third case ($h/B = 10$), the target was near the end and further outside of the potential core, respectively. Three different Reynolds numbers, 1780, 2960, and 4740 were maintained at the jet-exit in the experiment. The Reynolds numbers were defined based on the jet-exit velocity and the hydraulic diameter of the slot-jet, which can be shown to equal $2B$.

4.2. Problem parameters

The parametric investigations are conducted by carefully selecting a set of values for the important parameters relevant to this problem. These parameters are; *i*) the jet-exit Reynolds

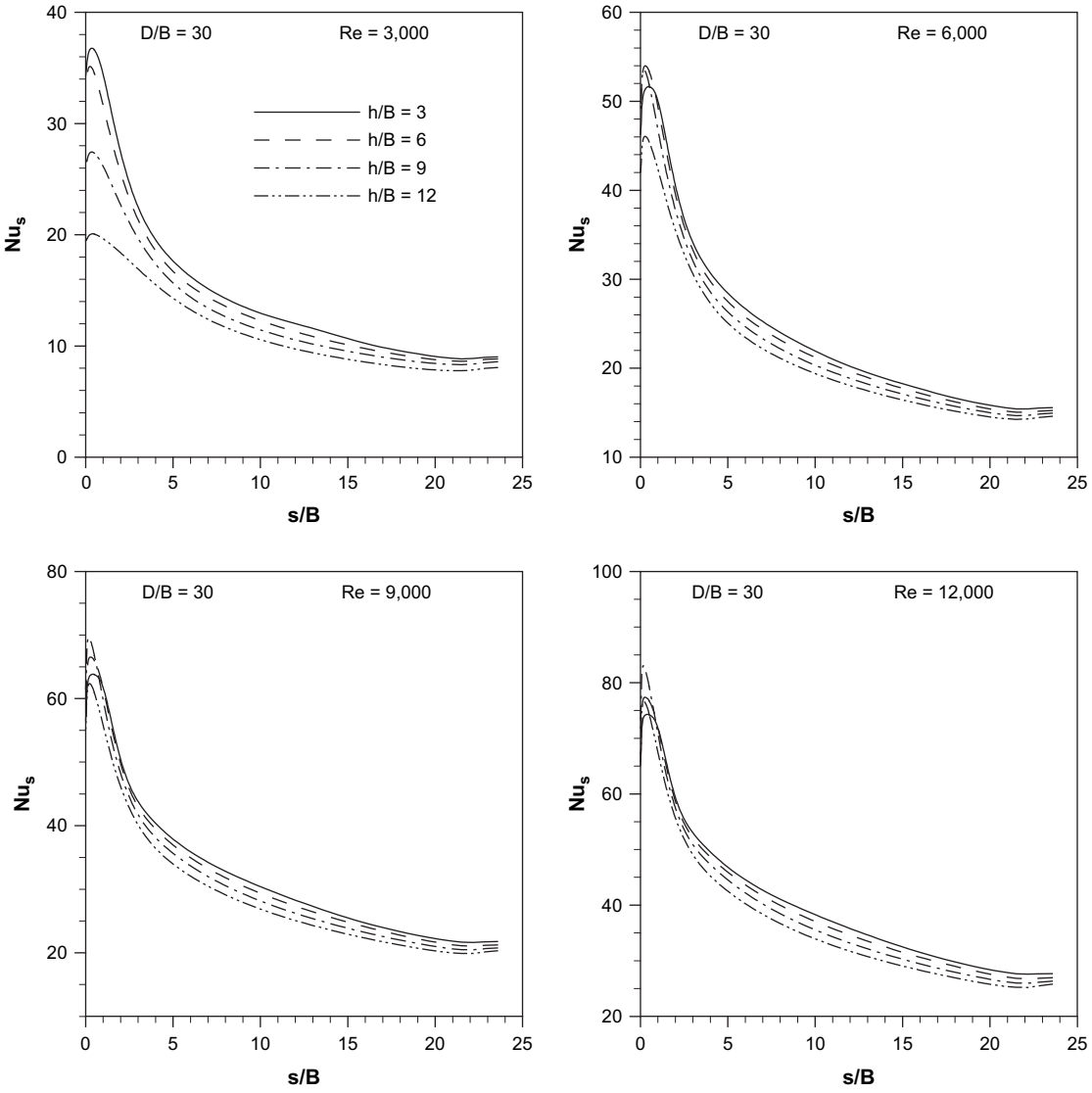

Fig. 8. Local Nusselt number variation along the heated concave surface for different Reynolds numbers for $D/B = 60$.

number, Re, *ii*) the normalized spacing between the nozzle exit and the impingement surface (h/B), and *iii*) the relative curvature of the impingement surface represented by the ratio of the surface diameter and the jet width, (D/B). The selected values of these parameters are; Re = 3000, 6000, 9000, and 12,000; $h/B = 3$, 6, 9, and 12; and $D/B = 30$, 40, 50, and 60. These result in a combination of 64 different cases of impinging flow on concave surfaces for which the computations are performed.

4.3. Fluid properties

Constant fluid properties of density, ρ (1.225 kg/m^3), dynamic viscosity, μ (1.7894×10^{-5} kg/m s), thermal conductivity, k (0.0242 W/m K), and specific heat at constant pressure, c_p (1006.43 N m/kg K) are used for all calculations. These values correspond to a Prandtl number, Pr, of 0.744.

4.4. Grid independence issues

A representative computational grid used for the impinging jet flows over semi-circular concave surface is also shown in Fig. 1(a). The grid is clustered towards the impingement surface and towards the free-jet region. Based on the geometrical symmetry of the flow, only half of the domain is computed. Fig. 1(b) shows the results of a typical grid independence study comparing the convergence of the local Nusselt number variation along the concave surface for different grid resolutions for the case of Re = 2960, $D/B = 30$, and $h/B = 10$. A close examination of the plots reveals that grid distribution in excess of 130×100 does not produce any significant change so this grid distribution is used for further computations of this case. Similarly, for each case, a systematic grid convergence study has been done to make sure proper grid resolution for grid independent results is selected and the y^+ value at the next to wall grid node is less than 1.

4.5. Boundary conditions

At the jet exit, velocity-inlet boundary condition is used with a velocity magnitude compatible to the jet-exit Reynolds number. A constant temperature of 300 K at the jet exit is also specified. On the concave wall, the no-slip wall boundary condition with constant heat flux value (5000 W/m^2) is set. At all other open

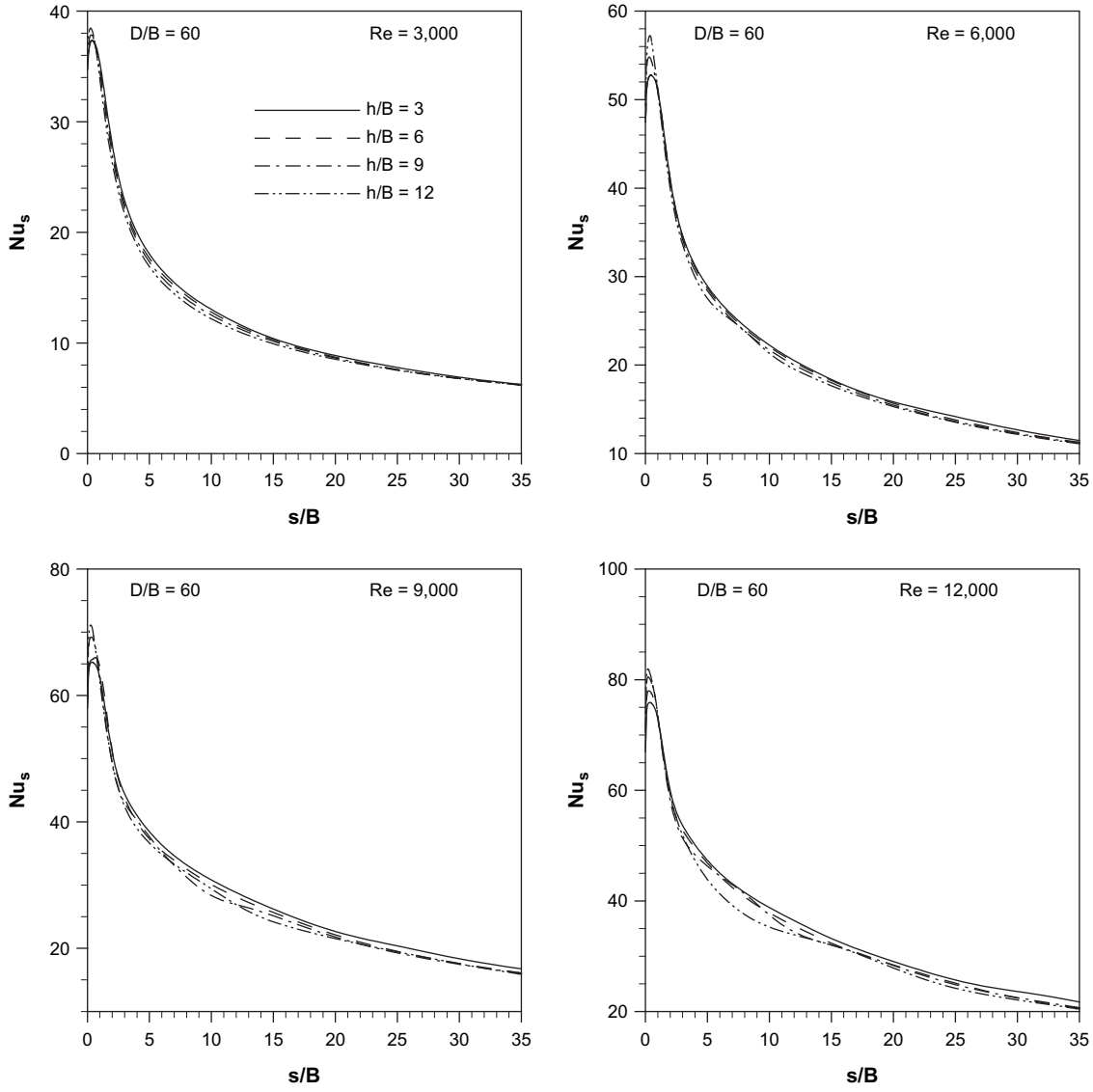

Fig. 9. Local Nusselt number variation along the heated concave surface for different Reynolds numbers for $D/B = 60$.

surfaces, constant pressure-outlet condition is used where the variables are extrapolated from inside.

4.6. Code validation

Before proceeding with the parametric study, a systematic code validation and performance evaluation of several turbulence models was conducted, the details of which are presented in a separate paper [28]. The turbulence models evaluated are; (*i*) the standard k–ε model [27], (*ii*) the RNG k–ε model [29], (*iii*) the realizable k–ε model [33], (*iv*) the SST k–ω model [34], and (*v*) the LRR Reynolds stress transport model [35]. Some excerpts of this evaluation are presented here to justify the rational of choosing the RNG k–ε model for the parametric study. Fig. 2 (reproduced from [28], Fig. 5) shows the comparison of the predicted local Nusselt number distribution along the heated concave surface against the experimental data of Choi et al. [18]. It can be seen that none of the models predict the Nusselt number distribution accurately for the entire length of the heated surface. Most of the models significantly under-predicts the Nusselt number in the wall-jet region ($s/B > 3$) away from the impingement region. The root mean square (RMS) error between the predicted Nusselt number distribution and the experimental data was calculated to quantify which model produced the least error. The RNG k–ε model and the SST k–ω model were found to have the least RMS error. Further comparison between the experimental and predicted hydrodynamic data for the decay of the jet centerline velocity by these two models as well as the Reynolds stress model is shown in Fig. 3 (reproduced from [28], Fig. 6). It can be seen that the RNG k–ε model predicts the best agreement to the experimental data for the jet centerline velocity. As such, the RNG k–ε model is selected for the intended parametric study, the results of which are presented next.

5. Results of the parametric study and discussion

The streamlines of the flow of jet impinging on a concave surface for some representative cases are presented in Fig. 4. The representative cases chosen are for $D/B = 30$, $h/B = 3$ and 12, and $\mathrm{Re} = 6000$ and 12,000. It can be seen in these streamline plots, that after impingement the jet gradually transforms into wall jet along the concave surface. The development of the boundary layer and the shear layer and their gradual spread is clearly discernible in

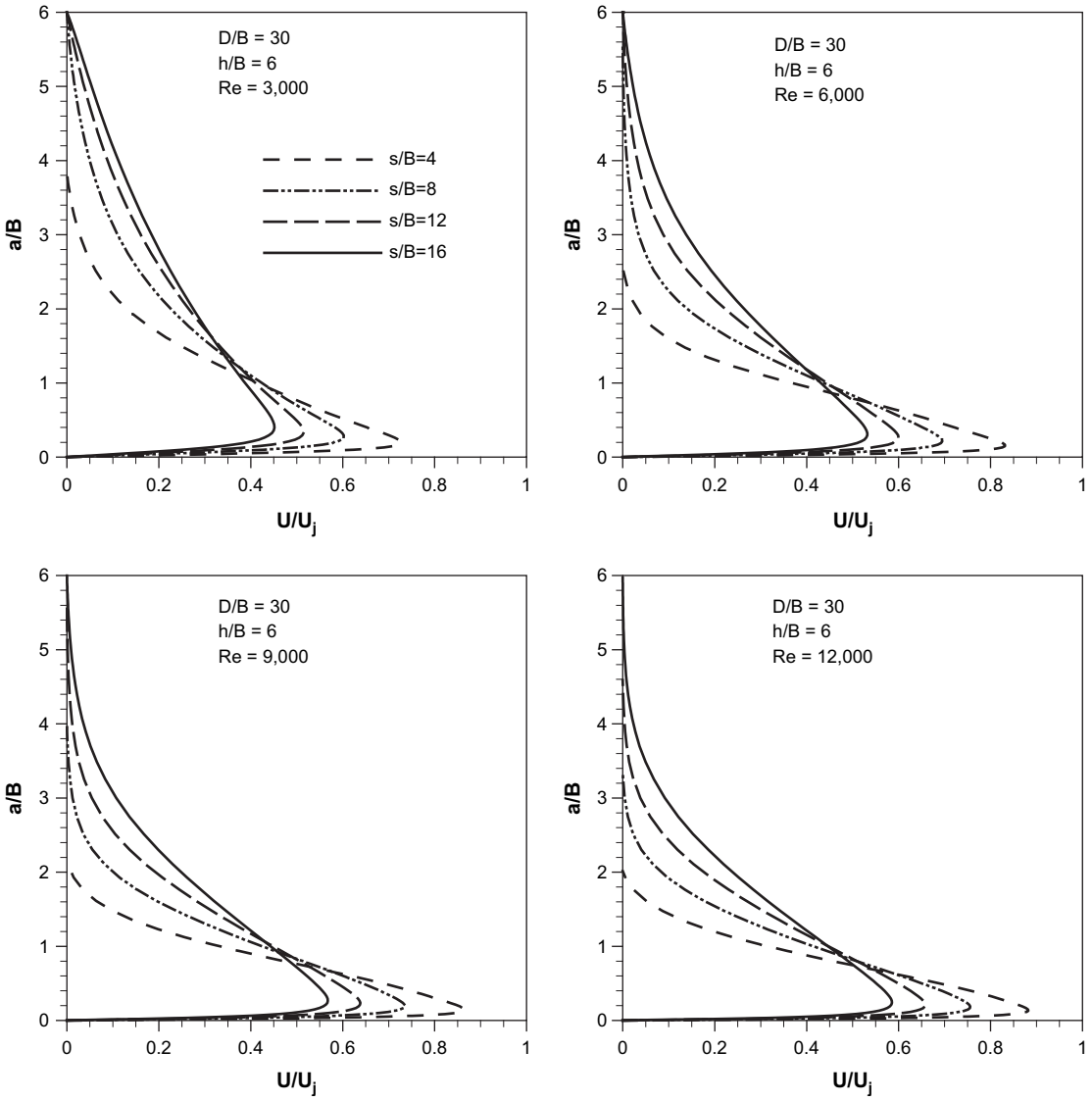

Fig. 10. Representative wall-jet velocity profiles at various circumferential locations.

these plots. The boundary and shear-layer thickness in the wall-jet region increases as the jet-to-surface spacing (h/B) is increased for a particular Reynolds number. The fluid entrainment at the free boundary of the domain is also depicted in these streamline plots. The entrainment seems to occur close to the jet when the separation (h/B) is smaller while for larger separation, the entrainment occurs almost over the entire free boundary. There is no flow separation or recirculation in the flow domain.

The isotherm plots for the same representative cases as in the preceding section are shown in Fig. 5. The isotherms are for the non-dimensional temperature θ defined as $(T-T_j)/\Delta T$ where T_j is the jet exit temperature and $\Delta T = q_w(2B)/k$, k being the thermal conductivity of the fluid. It can be seen from Fig. 5 that the thermal boundary layer thickness increases as we move away from the stagnation point along the circumferential direction. Very steep temperature gradients at the impingement region is noticed which is responsible for the high local Nusselt number there. Most of the fluid outside of the thermal boundary layer remains cold. Only a thin adjacent layer is affected by the constant heat flux condition at the concave surface.

While the streamline and isotherm plots display the general thermal hydraulic behavior of the convection process, they do not reveal any interesting feature of the flow. The plots of variation of the local Nusselt number along the heated concave surface are of more interest from the perspective of heat transfer effects for the problem. The local Nusselt number variation for a few representative cases are shown in Figs. 6 and 7 for $D/B = 30$ and 60, respectively. These plots show the significant effect of the jet-exit Reynolds number on the local Nusselt number variation at any combination of D/B and h/B. This can be attributed to the fact that the convection strength and turbulence level increases with increasing Reynolds number which in turn enhances heat transfer. The Nusselt number is highest in the impingement region ($s/B \sim 0$) at any configuration and at any Reynolds number. However, the peak of the Nusselt number occurs slightly downstream from the stagnation point ($s/B = 0$) from where the Nusselt number decreases monotonically. There are no predicted secondary maxima noticeable in the variation local Nusselt number even though there are experimental evidences that it occurs especially for impingement on flat surfaces when the impingement surface is

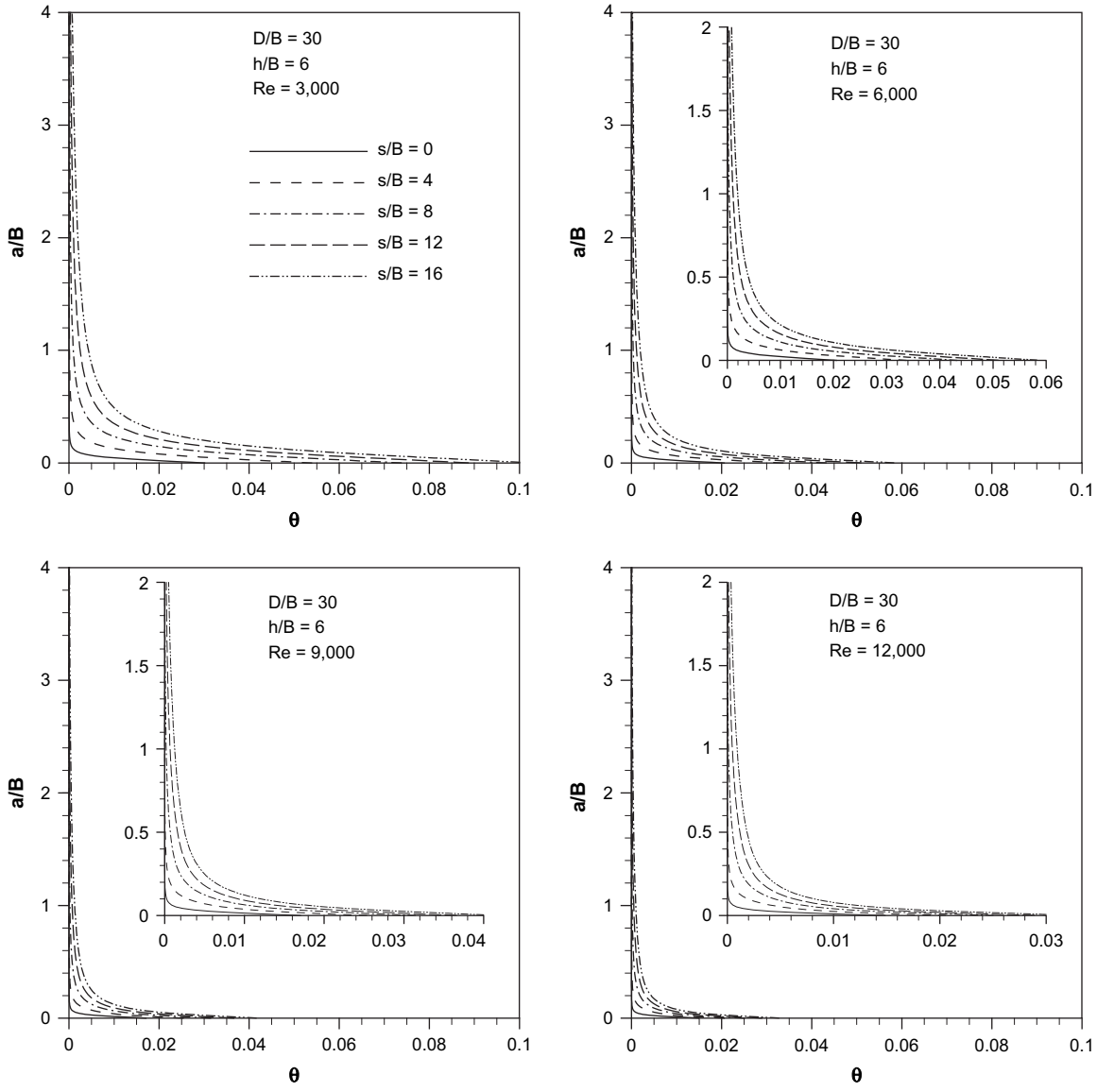

Fig. 11. Representative profiles of the non-dimensional temperature in the wall-jet at various circumferential locations.

within the potential core of the jet. The potential core of the jet where the turbulence intensity is very low and the flow is basically laminar, extends from the jet exit to about 5–8 jet widths downstream. When the impingement surface is placed close to the jet exit within the potential core, laminar to turbulent transitional flow occurs in the wall-jet regions at a downstream location close to the stagnation region which causes a secondary maximum in the heat transfer rate from the surface in this transitional region. When the impingement surface is placed outside of the potential core laminar to turbulent transition does not occur in the wall-jet region since the jet flow approaching the surface is already turbulent due to a large entrainment of ambient air to the jet flow. Thus, the secondary maximum smoothes out and both heat transfer rate and the skin friction decrease monotonically away from the stagnation point. The isotropic eddy-viscosity turbulence models, including the RNG k–ε model used in this study, are not capable of predicting transitional flow behavior which explains the absence of the predicted secondary maxima in the Nusselt number distribution.

In order to recognize the effect of jet-to-target spacing (h/B) on the Nusselt number at the heated concave surface, its distribution is again plotted in Figs. 8 and 9 for the same configurations as in Figs. 6 and 7 but now each subplot shows the distribution as h/B is gradually increased instead of the Reynolds number. The noticeable feature in these plots is that while the jet-to-target spacing has some significant effect on the Nusselt number at higher surface curvature ($D/B = 30$), its effect is much weaker at lower surface curvature ($D/B = 60$). It may be concluded from this trend that the effect of the jet-to-target spacing on the Nusselt number distribution diminishes as the surface curvature approaches the planer limit.

The hydrodynamic and thermal behavior of the wall-jet can be examined through velocity and temperature profiles within the wall-jet shear-layer. Representative plots of the velocity profiles for $D/B = 30$ and $h/B = 6$ at 4 different circumferential locations for various Reynolds numbers are shown in Fig. 10. The hydrodynamic shear layer thickness is increasing in the downstream direction (increasing s/B) at any specific Reynolds number. Also the maximum velocity in the profiles is diminishing while the location of the maxima is shifting away from the surface into the flow as s/B is increasing at any specific Reynolds number. Furthermore, the

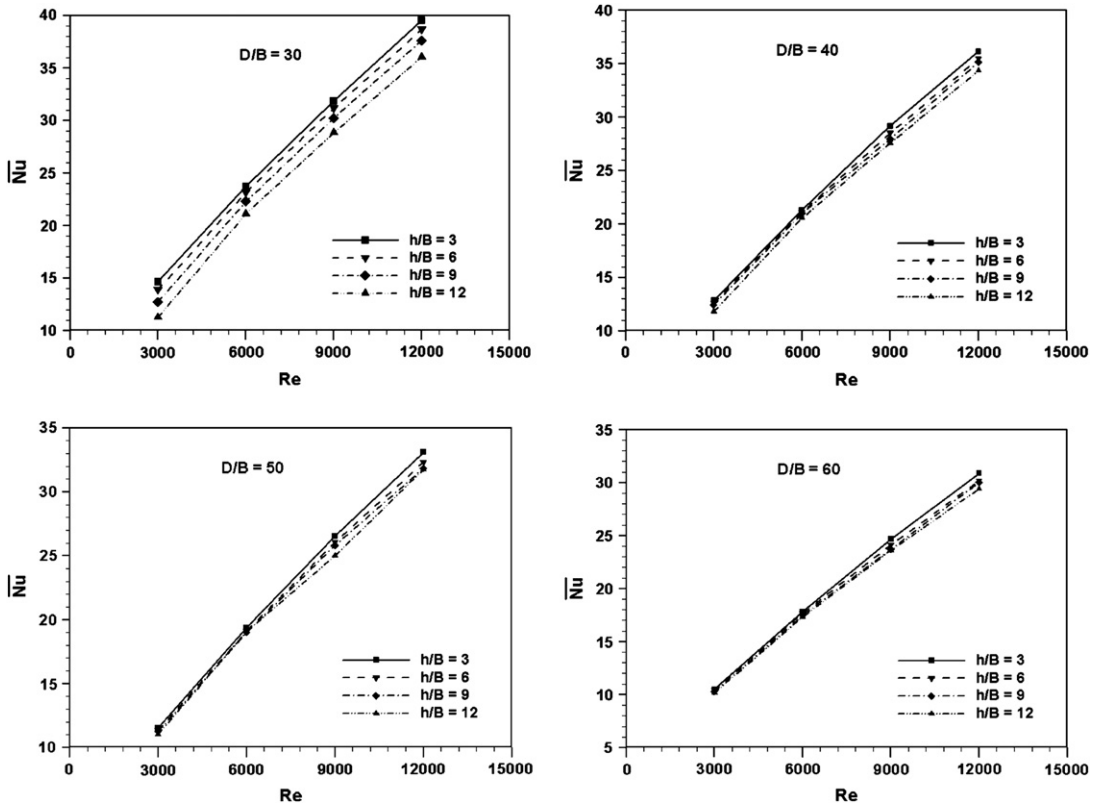

Fig. 12. Average Nusselt number at the heated concave surface as a function of the jet-exit Reynolds number.

wall-jet thickness decreases and the maximum velocity in the wall-jet increases with increasing Reynolds number at any specific circumferential location. Representative profiles of the non-dimensional temperature across the wall-jet for the same configurations as above at 5 different circumferential locations, including the stagnation point, for various Reynolds numbers are shown in Fig. 11. Magnified views of the profiles around the origin of the axes are shown as insets in some of these plots for clarity. Very steep temperature gradient at the surface and close to the stagnation point ($s/B = 0$) is noticed in these profiles at any specific Reynolds number, which explains the high value of the Nusselt number around the stagnation point. The temperature gradient at the surface gradually decreases as s/B increases indicating monotonic decrease of the Nusselt number in the circumferential direction. The thermal boundary layer is also very thin around the stagnation point which grows in the downstream direction. The thermal boundary layer thickness decreases with increasing Reynolds number at any specific circumferential location. These trends of velocity and temperature profiles seem to represent the correct convective heat transfer physics and conform to the expected wall-jet behavior.

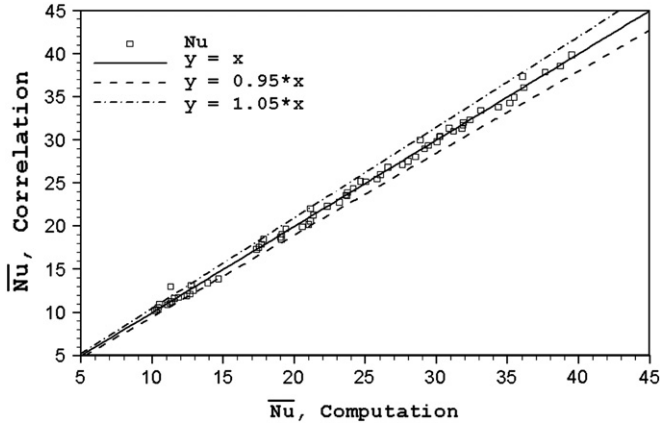

Fig. 13. Goodness of fit for the average Nusselt number correlation.

The overall effectiveness of the heat transfer process due to jet impingement on the heated concave surface can be quantified by the average Nusselt number which is obtained by integrating the local Nusselt number distribution along the surface and then dividing the integral by the total arc length of the impingement surface. This is calculated for all of the 64 configurations used in this study. The variation of the average Nusselt number is shown in Fig. 12 as a function of the Reynolds number for different combinations of D/B and h/B. The average Nusselt number increases almost linearly with Reynolds number for any specific combination of D/B and h/B. It is also more sensitive to the separation distance for higher relative curvature (lower values of D/B) but is somewhat insensitive as the surface curvature flattens (higher D/B values) especially at lower Reynolds number. This is consistent with the previous discussion on the local Nusselt number distribution at the heated surface.

From the results of the parametric study presented in the preceding sections, it is clear that the average Nusselt number at the curved surface is a function of (i) the jet-exit Reynolds number (Re), the relative curvature of the impingement surface (D/B), and the spacing between nozzle exit and impingement surface (h/B). A correlation expressing this functional relationship between the average Nusselt number and the other relevant parameters would be of interest and very desirable for design optimization. In order to derive this correlation a functional relationship of the form

$$\overline{\mathrm{Nu}} = C\mathrm{Re}^{m}(D/B)^{n}(h/B)^{p} \quad (10)$$

is assumed where, the constant C and the exponents m, n, and p are to be determined through a regression analysis of the 64 predicted data points for the different cases consisting of combinations of the above parameters. The desired functional relationship is obtained as

$$\overline{\mathrm{Nu}} = 0.107\mathrm{Re}^{0.761}(D/B)^{-0.346}(h/B)^{-0.047} \quad (11)$$

The separation parameter (h/B) has a rather weak effect on the average Nusselt number since its exponent is much smaller compared to that of the other parameters. Also the average Nusselt number varies inversely with the surface curvature and spacing (negative exponent) and directly with the Reynolds number (positive exponent). The goodness of fit for the derived correlation can be assessed by plotting the predicted average Nusselt numbers against those obtained from the derived correlation. This is done in Fig. 13 where most of the data points cluster around the straight line with a slope of 1. Two straight lines with slopes of 0.95 and 1.05 are drawn in Fig. 13 and most data points are within the bounds of these two lines which indicate that the correlation gives the average Nusselt number value within ±5% of the corresponding computed values. This asserts excellent goodness of fit for the derived correlation. The correlation should be valid for the range of parameters considered in its derivation such as $3000 < \mathrm{Re} < 12{,}000$, $3 < h/B < 12$, and $30 < D/B < 60$.

6. Conclusions

Parametric study of the turbulent slot-jet impingement heat transfer from concave cylindrical surfaces heated with constant heat flux condition is performed. The hydrodynamic and thermal field is computed using the RNG k–ε model with the two-layer enhanced wall treatment approach. The flow and geometric parameters include the Reynolds number at the jet exit (Re), the jet-to-target separation distance (h/B), and the relative surface curvature (D/B). Calculations are performed for 64 combinations of these parameters with the ultimate objective of deriving a correlation for the average Nusselt number at the heated surface as a function of these parameters. The results are presented in terms of the streamline and isotherm plots for representative cases, the local Nusselt number distributions along the concave heated surface, the variation of the average Nusselt number at the heated surface as a function of the various parameters, and the velocity and temperature profiles within the shear-layer of the wall-jet region.

The major conclusions of this parametric study are;

i) The Reynolds number has a significant effect on the heat transfer process. The local Nusselt number at the heated surface significantly increases at any particular circumferential location with increasing Reynolds number for any set of jet-to-target spacing and relative curvature.
ii) The local Nusselt number distribution starts with a high value at the stagnation point with a peak at a slightly offset location from the stagnation point and then quickly and monotonically decreases along the heated surface. No secondary peak is noticed in the local Nusselt number distribution even for the case when the surface is within the jet potential core ($h/B = 3$ and 6).
iii) The local Nusselt number distribution is not very sensitive to the jet-to-target spacing for higher relative curvature (D/B) values. This is due to the fact that the surface approaches to the planar limit as D/B increases.
iv) The surface curvature has significant effect on the local and average Nusselt number when the curvature is strong, i.e., at lower D/B values.
v) The average Nusselt number at the heated surface increases almost linearly with the Reynolds number. At higher D/B values, the average Nusselt number is insensitive to the jet-to-target spacing.
vi) The correlation for the average Nusselt number as a function of the parameters is derived for the range of the parameters considered.

References

[1] R.S. Bunker, D.E. Metzger, Local heat transfer in internally cooled turbine airfoil leading edge regions. Part I: impingement cooling without film coolant extraction, Journal of Turbomachinery 12 (1990) 451–458.
[2] C. Gau, C.M. Chung, Surface curvature effect on slot-air-jet impingement cooling flow and heat transfer process, Journal of Heat Transfer 113 (1991) 858–864.
[3] D.H. Lee, Y.S. Chung, D.S. Kim, Turbulent flow and heat transfer measurements on a curved surface with a fully developed round impinging jet, International Journal of Heat and Fluid Flow 18 (1997) 160–169.
[4] D.H. Lee, Y.S. Chung, M.G. Kim, Turbulent heat transfer from a convex hemispherical surface to a round impinging jet, International Journal of Heat and Mass Transfer 42 (1999) 1147–1156.
[5] Y. Kornblum, R.J. Goldstein, Jet impingement on semicylindrical concave and convex surfaces: part two–heat transfer, International Symposium on Physics of Heat Transfer in Boiling and Condensation, (1997) pp. 597–602.
[6] C. Cornaro, A.S. Fleischer, R.J. Goldstein, Flow visualization of a round jet impinging on cylindrical surfaces, Experimental Thermal and Fluid Science 20 (1999) 66–78.
[7] G.Y. Yang, M. Choi, J.S. Lee, A study of jet impingement cooling on the semi-circular concave surface: effects of two different nozzle configurations, In: Proceedings of the National Heat Transfer Conference, HTD-5, vol. 307 (1995) pp. 113–128.
[8] C. Cornaro, A.S. Fleischer, M. Rounds, R.J. Goldstein, Jet impingement cooling of a convex semi-cylindrical surface, International Journal of Thermal Sciences 40 (2001) 890–898.
[9] N. Kayansayan, S. Kucuka, Impingement cooling of a semi-cylindrical concave channel by confined slot-air-jet, Experimental Thermal and Fluid Science 25 (2001) 383–396.
[10] T.L. Chan, C.W. Leung, K. Jambunathan, S. Ashforth-Frost, Y. Zhou, M.H. Liu, Heat transfer characteristics of a slot jet impinging on a semi-circular convex surface, International Journal of Heat and Mass Transfer 45 (2002) 993–1006.
[11] H. Iacovides, D. Kounadis, B.E. Launder, J. Li, Z. Xu, Experimental study of the flow and thermal development of a row of cooling jets impinging on a rotating concave surface, Journal of Turbomachinery 127 (2005) 222–229.
[12] H. Eren, N. Celik, B. Yesilata, Nonlinear flow and heat transfer dynamics of a slot jet impinging on a slightly curved concave surface, International Communications in Heat and Mass Transfer 33 (2006) 364–371.
[13] C.H. Lee, K.B. Lim, S.H. Lee, Y.J. Yoon, N.W. Sung, A study of heat transfer characteristics of turbulent round jet impinging on an inclined concave surface using liquid crystal transient method, Experimental Thermal and Fluid Science 31 (2007) 559–565.
[14] S.W. Chang, S.F. Chiou, S.F. Chang, Heat transfer of impinging jet array over concave-dimpled surface with applications to cooling of electronic chipsets, Experimental Thermal and Fluid Science 31 (2007) 625–640.
[15] H. Eren, B. Yesilata, N. Celik, Nonlinear flow and heat transfer dynamics of a slot jet impinging on a slightly-curved surfaces, Applied Thermal Engineering 27 (2007) 2600–2608.
[16] G. Hu, L. Zhang, Experimental and numerical study of heat transfer with impinging circular jet on a convex hemispherical surface, Heat Transfer Engineering 28 (2007) 1008–1016.
[17] M. Fenot, E. Dorignac, J.J. Vullierme, An experimental study on hot round jets impinging on a concave surface, International Journal of Heat and Fluid Flow 29 (2008) 945–956.
[18] M. Choi, H.S. Yoo, G. Yang, J.S. Lee, D.K. Sohn, Measurement of impinging jet flow and heat transfer on a semi-circular concave surface, International Journal of Heat and Mass Transfer 43 (2000) 1811.
[19] Y.T. Yang, C.H. Hwang, Numerical simulations on the hydrodynamics of a turbulent slot jet impinging on a semi-cylindrical convex surface, Numerical Heat Transfer Part A 46 (2004) 995–1008.
[20] N. Souris, H. Liakos, Impinging jet cooling on concave surfaces, AIChE Journal 50 (2004) 1672–1683.
[21] S.E. Kim, D. Choudhury, A Near-wall Treatment Using Wall Functions Sensitized to Pressure Gradient, ASME FED, , In: Separated and Complex Flows, vol. 217, ASME, 1995.
[22] M. Frageau, F. Saeed, I. Paraschivoiu, Numerical heat transfer correlation for array of hot-air jets impinging on a 3-dimensional concave surface, Journal of Aircraft 42 (2005) 665–670.
[23] T.J. Craft, H. Iacovides, N.A. Mostafa, Modelling of three-dimensional jet array impingement and heat transfer on a concave surface, International Journal of Heat and Fluid Flow 29 (2008) 687–702.

[24] B.V.N.R. Kumar, B.V.S.S.S. Prasad, Computational flow and heat transfer of a row of circular jets impinging on a concave surface, Heat and Mass Transfer 44 (2008) 667–678.
[25] D. De Wrachien, G. Lorenzini, Modelling jet flow and losses in sprinkler irrigation: overview and perspective of a new approach, Biosystems Engineering 94 (2006) 297–309.
[26] 10 Cavendish Court NH 03766, www.fluent.com.
[27] B.E. Launder, D.B. Spalding, The numerical computation of turbulent flows, Computer Methods in Applied Mechanics and Engineering 3 (1974) 269–289.
[28] M.A.R. Sharif, K.K. Mothe, Evaluation of turbulence models in the prediction of heat transfer due to slot-jet impingement on plane and concave surfaces, Numerical Heat Transfer Part A 55 (2009) 273–294.
[29] V. Yakhot, S.A. Orszag, S. Thangam, T.B. Gatski, C.G. Speziale, Development of turbulence models for shear flows by a double expansion technique, Physics of Fluids A 4 (1992) 1510–1520.
[30] M. Wolfstein, The velocity and temperature distribution of one dimensional flow with turbulence augmentation and pressure gradient, International Journal of Heat and Mass Transfer 12 (1969) 301–318.
[31] N.Z. Ince, B.E. Launder, On the computation of buoyancy-driven turbulent flows in rectangular enclosures, International Journal of Heat and Fluid Flow 10 (1989) 110–117.
[32] S.V. Patankar, Numerical Heat Transfer and Fluid Flow, Hemisphere Publishing Corporation, 1980.
[33] T.H. Shih, W.W. Liou, A. Shabbir, Z. Yang, J. Zhu, A new k−ε eddy viscosity model for high Reynolds number turbulent flows, Computers & Fluids 24 (1995) 227–238.
[34] F.R. Menter, Two-equation eddy-viscosity turbulence models for engineering applications, AIAA Journal 32 (1994) 269–289.
[35] B.E. Launder, G.J. Reece, W. Rodi, Progress in the development of a reynolds-stress turbulent closure, Journal of Fluid Mechanics 68 (1975) 537–566.